PCCP

A theoretical study on the catalysis of Cu-exchanged zeolite for the decomposition of nitric oxide

Nobuo Tajima,* Masaki Hashimoto, Fuminori Toyama, Ahmed Mahmoud El-Nahas and Kimihiko Hirao

Department of Applied Chemistry, Graduate School of Engineering, University of Tokyo, Hongo 7-3-1, Bunkyo-ku, Tokyo 113-8656, Japan

Received 28th April 1999, Accepted 25th June 1999

The catalysis of Cu-exchanged zeolite for the direct decomposition of nitric oxide was investigated by hybrid density functional theory (B3LYP) using a molecular model of the active site. For reactions of two NO molecules over a Cu ion bound to the zeolite model (ZCu), the structures and energies of adsorption complexes and transition states were examined and compared with those of the corresponding reactions over an isolated Cu^+ and Cu atom and also reactions of free NO. The ZCu shows an enhanced catalytic activity compared with the isolated Cu^+. The ZCu and adsorbed molecules interact strongly in the transition state structures through π(d–p) bonding. Theory also suggests that the Cu atom has the potential to be a highly active catalyst for the NO decomposition reaction.

1 Introduction

Since the discovery of the catalytic activity of Cu-exchanged zeolite for the decomposition of nitric oxide (NO) into nitrogen and oxygen,[1] numerous attempts have been made to clarify the origin of the catalysis.[2–24] Although it is widely accepted that this reaction proceeds over Cu^+ ions supported by zeolite, little is understood about why the Cu site is so active. According to analyses of the active site structure using photoluminescence, UV, IR, EPR, ESR and X-ray techniques,[2–7] the Cu^+ is bound to the oxygen atoms of locally anionic Al tetrahedral sites of the aluminosilicate framework. This Cu site is entirely different from an isolated Cu^+ because the gas phase Cu^+ exhibits only low catalytic activity.[25]

One of the unique properties of this active site is the changeable oxidation state.[8–10] This implies that the Cu site can reversibly bind and release oxygen atoms formed by the cleaving of N–O bonds in the catalytic reaction. Another key property is the ability to activate N–O bonds, which is observed as the lowering of its stretching frequency compared with that in the gas phase.[9,11–13] This effect is explained by the formation of anionic NO in Cu(NO) and $Cu(NO)_2$ surface complexes due to electron transfers from the Cu sites.[12] The electronic and structural properties of the Cu complexes involved in NO decomposition have been studied theoretically.[14–24] Schneider *et al.*[14,15] and Brand *et al.*[16] have examined the interaction of NO molecules with Cu^+ where the Cu^+ is coordinated by water molecules to represent the zeolite environment. They showed that the Cu–NO binding energy and the strength of the N–O bond are strongly affected by the number of coordinated waters. These investigations support the contention that the chemical properties of Cu^+ are significantly controlled by the zeolite environment. Recently, Schneider *et al.*[17,18] have examined the energetics of the following reaction pathways, and showed that the Cu^+ bound to a zeolite model (ZCu) works more favorably as a catalyst than an isolated Cu^+:

$$ZCu + 2NO \rightarrow ZCuO + N_2O \rightarrow ZCu + O_2 + N_2 \quad (1)$$

$$ZCuO + NO \rightarrow ZCuNO_2,\ ZCuO + NO_2 \rightarrow ZCu + NO + O_2 \quad (2)$$

$$ZCu + N_2O \rightarrow ZCuO + N_2 \quad (3)$$

Their conclusion so far is that the reaction (1) is plausible.[18]

In this study, we investigated theoretically the interactions of zeolite bound Cu ion with reactants and intermediates in the catalytic cycles of NO decomposition to achieve a further understanding of the mechanism of the activation of Cu ion by the zeolite framework. We studied the structures in reaction path (1) using different cluster models of the active site and different density functional methods from those of previous studies. We report in detail the change in the bonding nature of Cu^+ with adsorbed molecules due to cluster support.

2 Computational methods

The interactions of ZCu with adsorbates in the equilibrium and transition state structures in reactions (1) were investigated. We compared the results with those of the corresponding reactions of free NO molecules and also those over an isolated Cu^+ and Cu atom (Cu^0). The system with Cu^0 is considered because many previous theoretical studies[14–21] have shown that Cu^+ becomes more or less negative on the zeolite clusters, which implies that the catalytic nature of ZCu may be close to that of Cu^0. The reaction paths are assumed to lie on the triplet potential energy surfaces, except that we applied a doublet for the reactions over the Cu^0.

The zeolite surface is modeled by the atom cluster (SiH_3)–O–$Al(OH)_2$–O–$(SiH_3)^-$ as shown in Fig. 1. This cluster is different from that used in previous calculations,[17,18] *i.e.*, $Al(OH)_4^-$. This model size was chosen because it is regarded as the smallest limit that guarantees a realistic description of the surface complex for the case of H-form zeolite.[26] This cluster is picked out from the 10-ring structure of the ZSM-5 zeolite.[20] The Si atom of the central tetrahedral site (T-12 site[27]) is substituted with an Al atom, and the terminal dangling bonds are satisfied by H atoms. The experimentally observed atom positions[27] are employed for the Si and the hydroxyl oxygens, and the geometry of the remaining atoms is optimized. In the calculations of complexes on this cluster model, the determined geometry is fixed except for the O–Al–O part around the Cu ion. Partial use of the experimental geometries here is not intended to model a particular

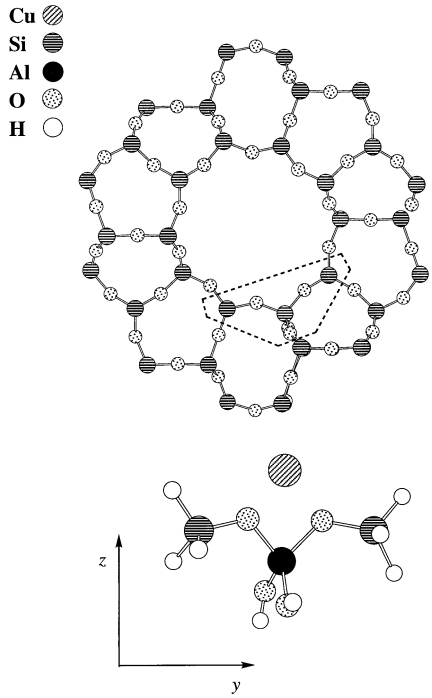

Fig. 1 View of the 10-ring structure of ZSM-5 zeolite and the cluster model of the active site. The central T-site of the cluster is the T12 site of ZSM-5.

active site but to keep the cluster geometry realistic as a zeolite surface.

Owing to the use of fixed atoms, the equilibrium and transition state structures are located as stationary points with respect to the coordinates of free atoms, and accordingly their natures are determined by diagonalizing the corresponding parts of the force constant matrices. The connectivities of the stationary points were verified by locating equilibrium structures from transition state structures through conventional optimization for cluster-containing systems, and by the intrinsic reaction path (IRC) following the methods for the other systems.

All calculations are carried out by Becke's three parameter hybrid density functional method[28] with the Lee–Yang–Parr correlation functional (B3LYP).[29] The cc-pVDZ[30] basis sets are used for N and O atoms and the (4s)/[1s] set in the cc-pVDZ is used for hydrogen atoms. For Al, Si and Cu atoms, the basis sets of double-zeta quality with effective core potentials to represent 10 electrons (1s–2p) proposed by Hay and Wadt[31] are used. The electronic structures of complexes are investigated by natural population analysis.[32] The calculations are performed using the GAUSSIAN 94 program package.[33]

Use of the B3LYP method is determined by checking the accuracy with the basis sets described above for the geometries and bond-dissociation energies of molecules to be involved in the reaction, N_2, O_2, NO, N_2O, NO_2, CuO and $(NO)_2$. Comparisons are made with the density functional method using Becke's exchange[34] with Perdew's correlation[35] functional (BP86) and the second order Møller–Plesset (MP2) method[36] where electrons except 1s of N and O atoms are correlated. $(NO)_2$ appears in the reaction paths of NO decomposition as described in the next section, but it is difficult to perform reliable calculations to describe the weak bond due to the π^*–π^* interactions.[37,38] Experimental uncertainty exists for this molecule as to whether the ground electronic state is singlet or triplet, while the structure is analyzed to be in the C_{2v} *cis* form[39,40] having very weak N–N bonding of about 2 kcal mol^{-1}.[41,42] Calculations are performed for both states and the results of the more stable one should be compared with the experimental values.

The results in Table 1 indicate that the B3LYP method gives good agreement with experimental values.[43] The calculated errors are within a few kcal mol^{-1} in energy and few

Table 1 Dissociation energies and structures of molecules involved in NO decomposition[a]

	State		B3LYP	BP86	MP2	Experiment
Dissociation energies—						
N_2	$^1\Sigma_g^+$	D(N–N)	219.3	238.6	209.8	225.0[b]
O_2	$^3\Sigma_g^-$	D(O–O)	121.3	142.9	114.0	118.0[b]
NO	$^2\Pi$	D(N–O)	149.8	170.2	133.7	149.8[b]
N_2O	$^1\Sigma^+$	D(NN–O)	44.6	67.4	39.4	38.7[b]
		D(N–NO)	114.1	135.8	115.4	113.7[b]
		D(N–N–O)	263.9	306.0	249.1	263.5[b]
NO_2	$^2A_1$	D(O–NO)	74.6	96.0	73.8	71.8[b]
		D(N–O_2)	103.2	123.2	96.7	113.8[b]
ONNO						2.0[c]
	$^1A_1$	D(ON–NO)	−2.9	10.2	9.5	
	$^3B_1$	D(ON–NO)	−0.2	15.5	0.5	
CuO	$^2\Pi$	D(Cu–O)	59.2	74.8	48.3	62.2[b]
Structures—						
N_2	$^1\Sigma_g^+$	r(N–N)	1.104	1.117	1.130	1.098[b]
O_2	$^3\Sigma_g^-$	r(O–O)	1.209	1.226	1.232	1.208[b]
NO	$^2\Pi$	r(N–O)	1.154	1.168	1.140	1.151[b]
N_2O	$^1\Sigma^+$	r(N–N)	1.134	1.151	1.172	1.128[b]
		r(N–O)	1.188	1.196	1.185	1.184[b]
NO_2	$^2A_1$	r(O–N)	1.199	1.214	1.208	1.193[b]
		θ(ONO)	134.2	133.6	134.1	134.1[b]
ONNO						
	$^tA_1$	r(O–N)	1.155	1.168	1.178	1.152[d]
		r(N–N)	1.995	2.065	2.221	2.263[d]
		θ(ONN)	99.6	98.2	91.0	97.2[d]
	$^3B_1$	r(O–N)	1.158	1.171	1.175	
		r(N–N)	1.949	1.999	2.311	
		θ(ONN)	110.4	110.9	94.2	
CuO	$^2\Pi$	r(Cu–O)	1.764	1.735	1.803	1.724[b]

[a] Bond lengths r in Å and bond angles θ in degrees. Dissociation energies D in kcal mol^{-1}. The dissociation energies are corrected for zero point energies. Basis sets: N and O, cc-pVDZ;[30] Cu, valence double-zeta basis set with effective core potential (1s–2p core) proposed by Hay and Wadt.[31] [b] Ref. 43. [c] Refs. 41 and 42. [d] Ref. 40.

hundred Å in bond distance, except for the structure of $(NO)_2$. The accuracy is comparable to that of the MP2 method. On the other hand, the BP86 method, which has frequently been used in studies of ZCu–NO systems,[14,15,17,18] shows poor agreement with experiment, especially concerning the energies. This functional tends to overestimate binding energies by a few tens of kcal mol^{-1}. Accurate binding energies are essential for a proper description of the catalytic effects of the Cu active site and, therefore, the BP86 method is not appropriate for our study.

In the B3LYP method, the ground state of $(NO)_2$ is calculated as $^3B_1$. The predicted dissociation energy is close to the experimental estimate. The N–N bond length deviates significantly from the experimental value,[40] but it should be understood by the difficulty of locating accurate geometries on a very flat energy curve. Recently, Duarte *et al.*[38] reported that any density functional method predicts the triplet ($^3B_1$) as the ground state with substantially overestimated binding energies. It seems that the hybrid of the Hartree–Fock and the density functional scheme in the B3LYP method contributes to reducing such an overestimate. This method may still have more or less inaccuracy, but it is expected that this method will avoid serious errors.

3 Results and discussion

3.1 Reaction of free NO

Fig. 2 shows the energy diagram of the reactions of free NO. Three reaction pathways (I)–(III) are examined.

Pathway (I) is found to be the most energetically preferred within this study. This reaction consists of two elementary steps, first the cleavage of the N–O bond in NO dimer to produce N_2O and O and second the cleavage of the N–O bond in N_2O to produce N_2 and O_2. The first reaction is the rate determining step and the second step proceeds faster than the first. The activation energy of about 50 kcal mol^{-1} for the first reaction indicates that the gas phase decomposition is a high energy process. Nevertheless, the energy required to cleave NO bond is much lower than that of a single NO molecule of about 150 kcal mol^{-1}. In this scheme, the $(NO)_2$ is a precursor of N–N bond formation, but the N–N bond is too weak to activate the N–O bond.

In reaction pathway (II) the two N–O bonds dissociate simultaneously to produce N–N and O–O bonds, whereas in pathway (III) the two NO molecules react to form NO_2 and N as intermediates. The transition state for reaction (II) is searched for under C_2 symmetry, but the calculated structure **SP-1** is a saddle point of third order with very high energy (122.0 kcal mol^{-1}). The energy for reaction (III) is calculated as 75.3 kcal mol^{-1}. These results indicate that reactions (II) and (III) are less preferred than (I). It can be confirmed that reaction (I) is the most probable one for the reactions of two NO molecules.

The reaction $2NO \rightarrow N_2 + O_2$ is exothermic. However, the reaction does not proceed since the barrier is too high in the gas phase. The high energies of the transition states and intermediates originate from the unstable isolated atomic-like oxygen O1. Hence the reaction could proceed if this atomic-like oxygen is stabilized with the help of a catalyst.

3.2 Reaction over Cu^+

The decomposition of NO over Cu^+ proceeds in the same way as in the case of free NO (Fig. 3); steps **1**, **TS-1** and **TS-2** correspond to those of the free NO and the other steps such as **1a**, **2a**, **2b**, **3a** and **3b** are additional adsorbed structures due to the presence of Cu^+. The Cu^+ affects the reactivity by stabilizing each step through the interactions with adsorbates.

The production of N_2O in the first reaction (from **1** to **2a**) seems to be easier than that for the free NO because the activation energy is lowered in the presence of Cu^+ compared with that for free NO (37.5 and 52.1 kcal mol^{-1}, respectively). The decrease in the activation energy is expected from the preceding adsorbed structure **1** (Cu^+ONNO), where the interaction between the two NO is stronger than that of the free NO, as indicated by the binding energy of two NO and the N–O bond length (Fig. 3). According to an experimental study,[25] N_2O production from NO is not very feasible even over an isolated Cu^+. We believe that this can be explained by the presence of adsorbed structures **1a′** (Cu^+NO) and **1′**

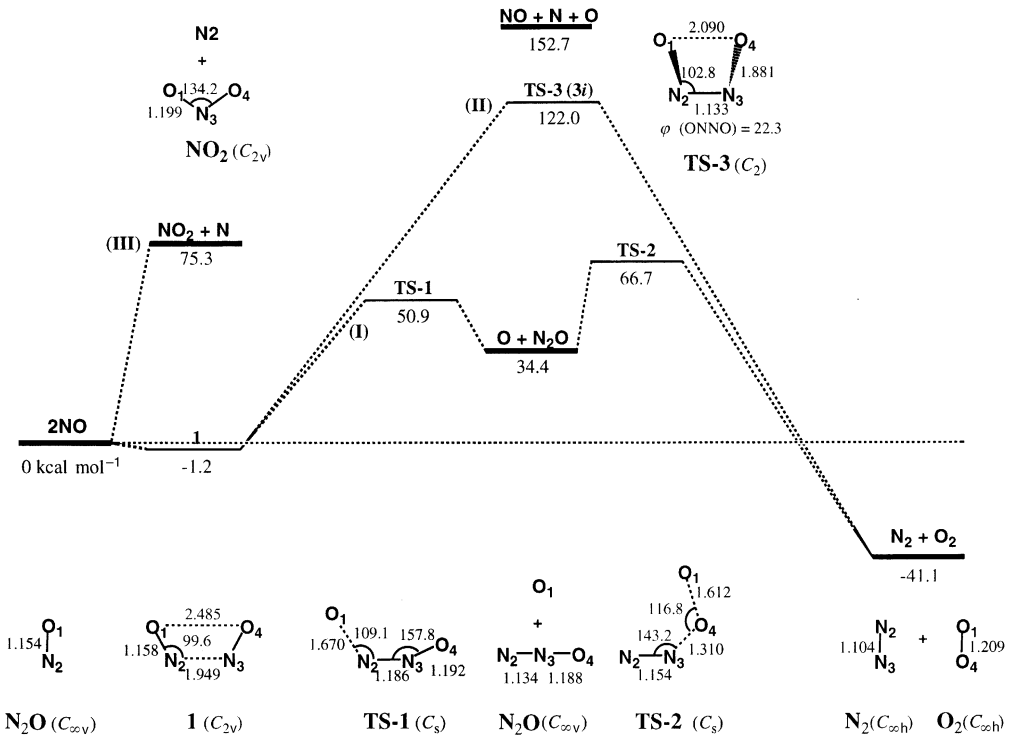

Fig. 2 Energy diagram of the reaction $2NO \rightarrow N_2 + O_2$. Energies (in kcal mol^{-1}) are relative to the dissociation limit of two NO. Bond lengths and angles are in ångstroms and degrees, respectively.

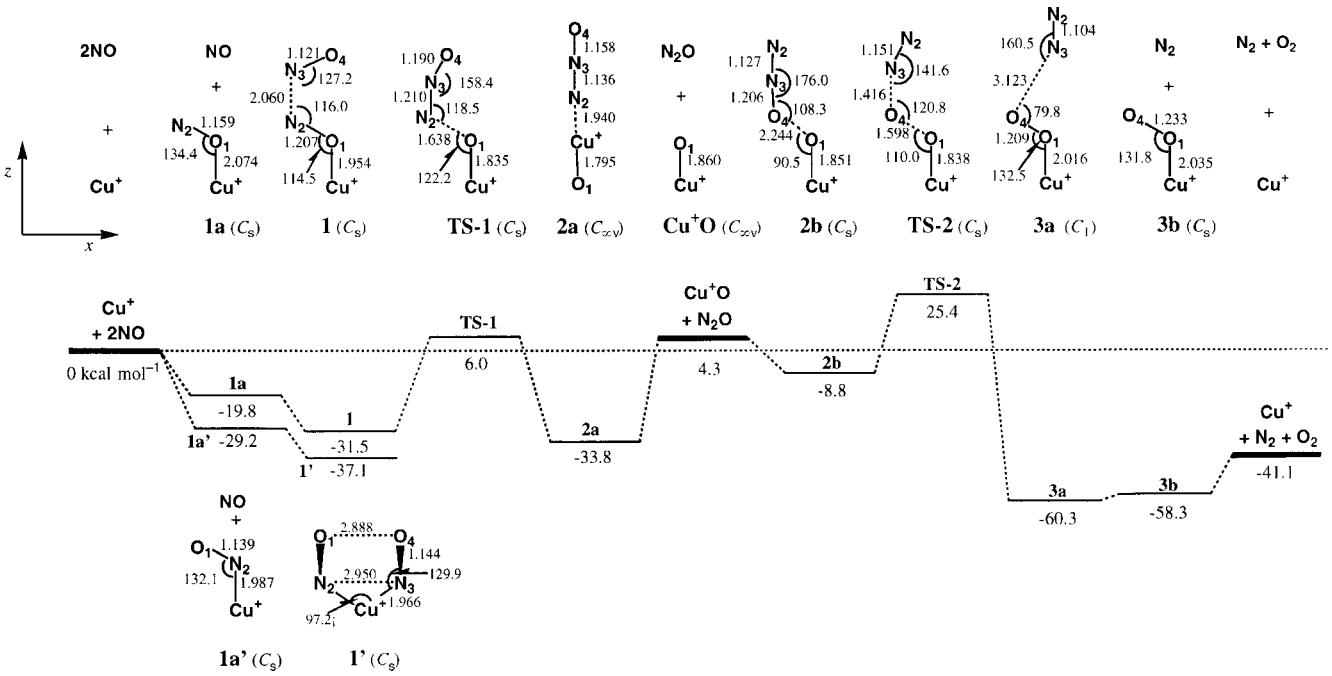

Fig. 3 Energy diagram of the reaction $2NO \rightarrow N_2 + O_2$ over Cu^+. Energies (in kcal mol^{-1}) are relative to the dissociation limit of two NO and Cu^+. Bond lengths and angles are in ångstroms and degrees, respectively.

$[Cu^+(NO)_2]$, which are stable isomers of **1a** (Cu^+ON) and **1** (Cu^+ONNO).

After the first reaction, the N_2O desorbs from the Cu^+ and then the second elementary reaction occurs through transition state **TS-2** to form N_2 and O_2. The precursor of the second reaction **2b** ($Cu^+O\cdots ONN$) is unstable compared with the isomer **2a** ($ONNCu^+O$). Therefore, the net activation energy for the second reaction should be the energy difference between **2a** and **TS-2**. Since much more energy is required for the transition from **2a** to **TS-2** than for the first reaction, the second reaction will be the rate determining step.

The interactions between the Cu^+ and adsorbed molecules seem to be mainly electrostatic because the net charges of the Cu^+ are maintained within the range $+0.92$–1.05 (net charges and electron populations are available as Supplementary Data†). The mixing in the orbitals between the Cu^+ and adsorbates is small, which confirms the non-covalent nature of the bonding. Deviations in the $Cu^+(3d)$ and $Cu^+(4s)$ populations from the $Cu^+(d^{10}s^0)$ occupation are observed. These population changes are small (0.04–0.11*e*) in structures **1a**, **1**, **3a** and **3b**, but relatively large (0.16–0.36*e*) in going from **TS-1** to **TS-2**. The decrease in the 3d population results from the mixing of the $3d_{z^2}$ with the 4s and with the in-plane orbitals of adsorbates (the *x*,*y*,*z* coordinate system is given in Fig. 3), *i.e.*, the π^* orbital of NO in **1a** and **1**, the p_z orbital of O1 in **TS-1**–**TS-2** and the π^* orbital of O_2 in **3a** and **3b**. In structures **TS-1**–**TS-2**, population changes in $3d_{yz}$ are pronounced (0.10–0.14*e*). The $3d_{yz}$ mixes with the out-of-plane orbitals of the adsorbates composed mainly of the p_y of O1.

3.3 Reaction over Cu^0

Fig. 4 displays the energy diagram of the NO decomposition over Cu^0. The calculated structures on this reaction path are different from those over Cu^+, where the second transition state **TS-2** is cyclic, and the adsorbed structure **2b** is absent. A transition-state structure of the type **TS-2** in the case of Cu^+ is obtained, but the energy is higher than that for **TS-2** by 7.0 kcal mol^{-1}.

The reaction over Cu^0 is characterized by low energies of the two transition states. The energies of the first and second transition states are lowered by 17.1 and 24.4 kcal mol^{-1}, respectively, compared with those over Cu^+. The activation energy of only 8.2 kcal mol^{-1} for the first reaction suggests that this reaction is very fast. Such high catalytic activity should be ascribed to the ability of Cu^0 to activate NO; the N–O bond of the adsorbed structure **1a** is significantly lengthened, and the elongation is very large for the adsorbed structure **1** (Fig. 4). As for the second transition state **TS-2**, two-site bonding of the adsorbates to Cu^0 in the cyclic structure partially accounts for the low energy. The remaining stabilization comes from the strong oxygen affinity of Cu^0, which is indicated in the short Cu–O bond in almost every structure. Nevertheless, the second reaction seems to be a difficult process because the activation from **2a** to **TS-2** demands very high energy.

The main feature of the interactions in the complexes is substantial charge transfers from $Cu^0(d^{10}s^1)$ to adsorbates. Except for the structure **1**, about 0.39–0.64*e* transfers from 4s, and 0.13–0.30*e* from 3d. The decrease in the 3d population comes mainly from $3d_{z^2}$(0.07–0.16*e*) (the *x*,*y*,*z* coordinate system is given in Fig. 4), and slightly from $3d_{xz}$ (0.00–0.08*e*). In these structures, the out-of-plane orbitals of the adsorbates, $O(2p_y)$ in structures **TS-1**–**TS-2** and $O_2(\pi_y^*)$ in **3a** and **3b**, are entirely filled. Instead, the in-plane orbitals of the adsorbates, $O(2p_z)$ in **TS-1**–**TS-2** and $O_2(\pi_x^*)$ in **3a** and **3b**, are partially occupied. The mixing of these in-plane orbitals with the $3d_{z^2}$ and the 4s orbitals mainly accounts for these electron transfers. There also is weak mixing of the $3d_{xz}$ with the in-plane orbitals of the adsorbate, $O(2p_x)$ in **TS-1**–**TS-2** and $O_2(\pi_x^*)$ in **3a** and **3b**. Hence interaction between the Cu^0 and adsorbates is a composite of partially ionic and partially covalent bonding.

3.4 Reaction over ZCu

Fig. 5 depicts the energy diagram of the NO decomposition over ZCu. The structures in this reaction path are not very different from those for the isolated Cu^+, except structures **2a**

† Supplementary material available (SUP 57593, 5 pp.), deposited with the British Library. Details are available from the Editorial Office. For direct electronic access see http://www.rsc.org/suppdata/cp/1999/3823.

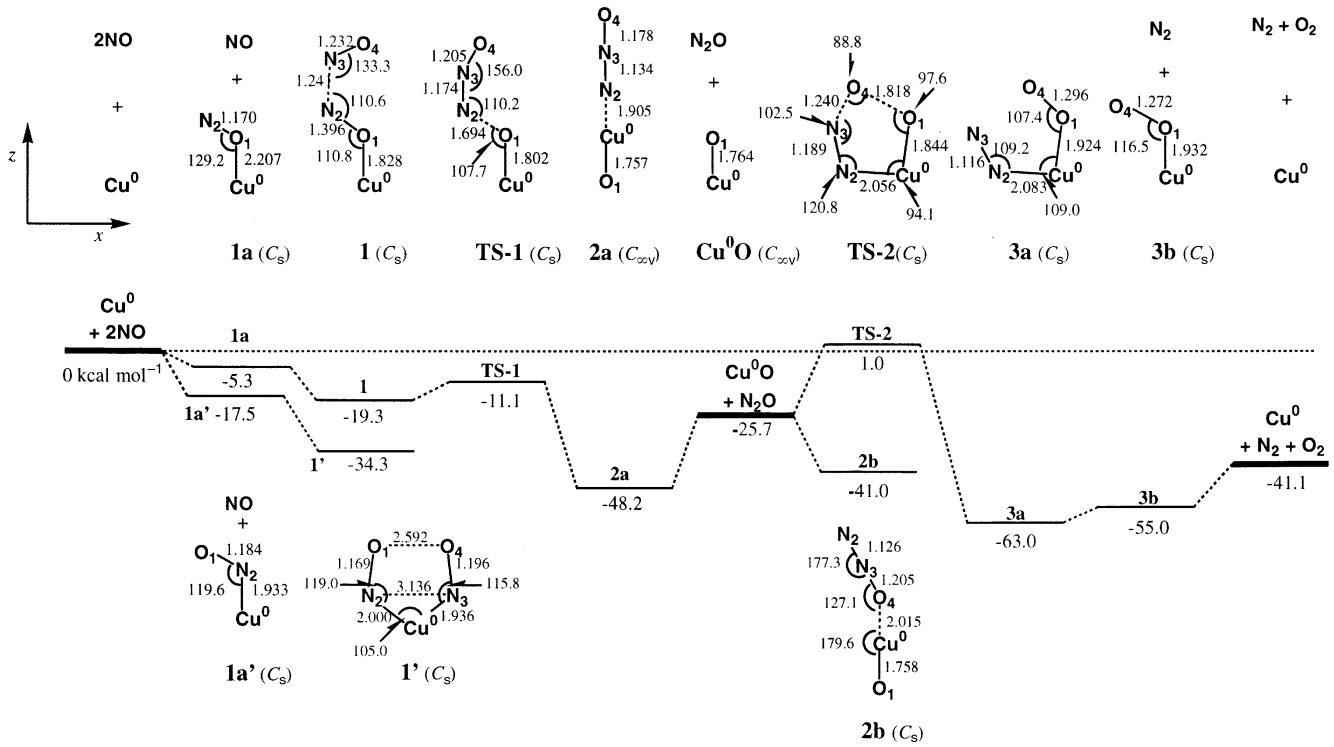

Fig. 4 Energy diagram of the reaction $2NO \rightarrow N_2 + O_2$ over Cu^0. Energies (in kcal mol^{-1}) are relative to the dissociation limit of two NO and Cu^0. Bond lengths and angles are in ångstroms and degrees, respectively.

and **2b**. In **2a**, the linear structure observed in the isolated Cu^+ system is inhibited because of the presence of the cluster oxygens (Oz), and instead a tetrahedral structure is produced. In **2b**, N_2O attaches to Cu^+ directly rather than to O1, and as a consequence a tetrahedral structure is produced around the Cu^+. The tetrahedral structure is known as the most preferred coordination of four ligands around Cu^+.[44] In the other structures, the Cu^+ and adsorbates form almost planar structures which are perpendicular to the Oz–Cu–Oz-plane. This energy diagram is compared with those for the free NO molecules and NO with Cu^+ and Cu^0 in Fig. 6.

The energy diagram indicates that ZCu effectively catalyzes the NO decomposition. The activation energy for the first reaction (from **1** to **TS-1**) amounts to only 18.2 kcal mol^{-1}, and that for the second reaction (from **2b** to **TS-2**) is calculated as 39.2 kcal mol^{-1}. The energy barrier of the rate determining reaction is thereby lowered by 12.9 kcal mol^{-1} compared with the reaction of free NO. The low energy

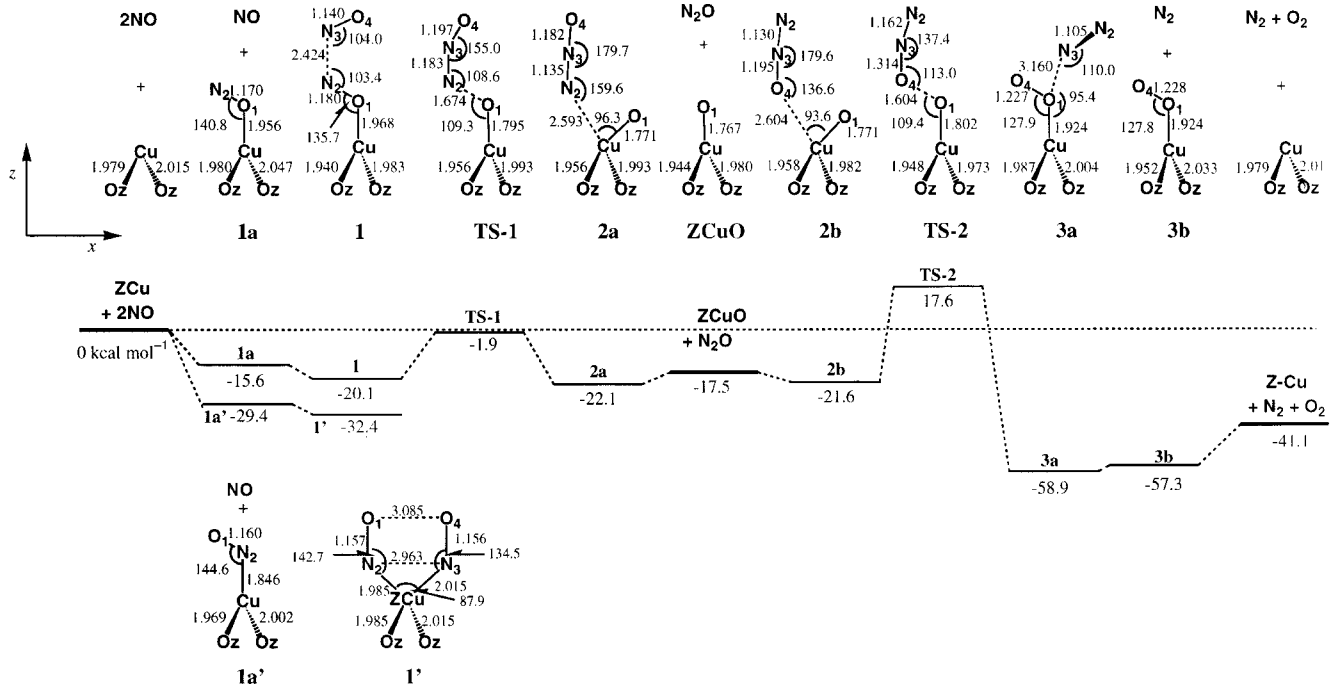

Fig. 5 Energy diagram of the reaction $2NO \rightarrow N_2 + O_2$ over ZCu. The symbol Oz represents the oxygen in the cluster model (see Fig. 1). The Oz–Cu–Oz planes are almost perpendicular to the *x*–*z* plane. Energies (in kcal mol^{-1}) are relative to the dissociation limit of two NO and ZCu. Bond lengths and angles are in ångstroms and degrees, respectively.

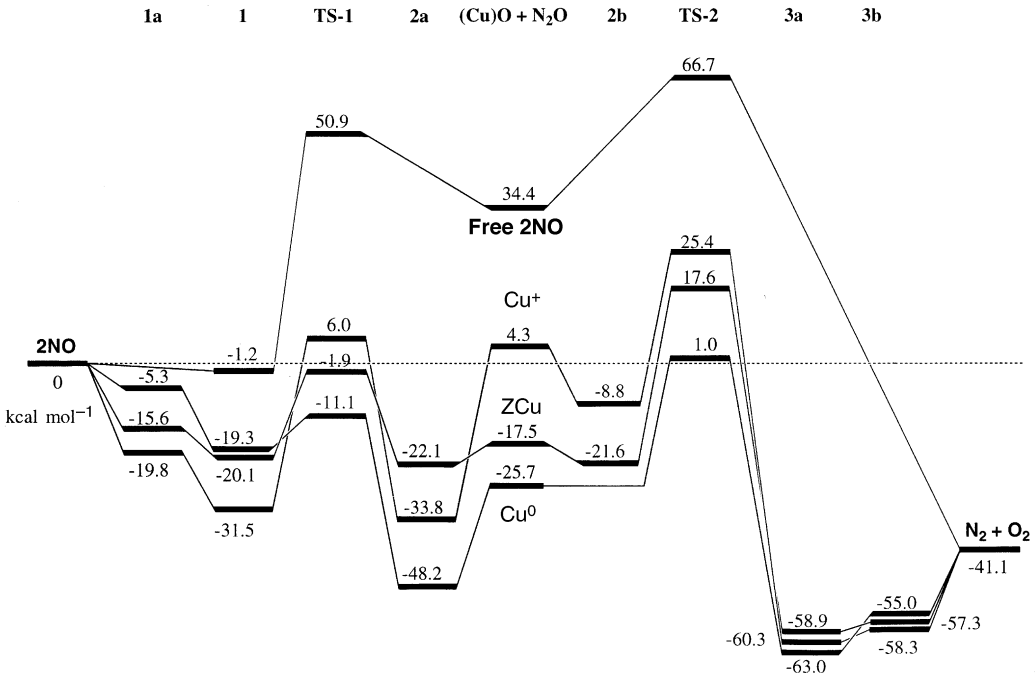

Fig. 6 Comparison of energy diagrams of NO decompositions: reactions of free 2NO (Fig. 2) and those over Cu^+ (Fig. 3), Cu^0 (Fig. 4) and ZCu (Fig. 5). See the figures mentioned for structures.

barrier of the first reaction indicates that it proceeds even at low temperatures. The relatively high energy barrier of the second reaction implies that this process is activated at elevated temperatures, or it may compete with other feasible reactions. It is known experimentally[1,10,12] that the intermediate product due to the first reaction, N_2O, is detectable at temperatures below that of the maximum activity (about 800 K), and that the final product O_2 is not produced stoichiometrically because of the formation of NO_2 by-product. The energy diagram of the ZCu seems consistent with these experimental findings.[1,10,12]

The energy of each step is compared with that calculated by Schneider *et al.*[17,18] using different zeolite cluster $Al(OH)_4^-$ and different density functional methods (BP86) in Table 2. Our energies are larger than their results by about 10–20 kcal mol^{-1} as a whole. The energy barrier of the first reaction is larger than their values by about 10 kcal mol^{-1}, while that of the second reaction is comparable. We also calculated the energies of these steps by the BP86 functional with the cluster model shown in Fig. 1. Our BP86 energies are smaller than the B3LYP energies, and are close to those of Schneider *et al.*[17,18] for most of the structures. It can be concluded that the difference between our energies and their values can mainly be ascribed to the use of different functionals.

By comparing the energy diagram of ZCu with that of the isolated Cu^+, it is evident that the ZCu is a more active catalyst. The enhanced catalytic effect results from the energy decreases in the transition-state structures **TS-1** and **TS-2** by 7.9 and 7.8 kcal mol^{-1}, respectively, compared with the reaction over the isolated Cu^+, and from the energy increases in the adsorbed structures **1** and **2a** by 11.4 and 11.7 kcal mol^{-1}, respectively. Certainly, as a result of these energy changes, the high energy process observed for the Cu^+ (transition from **2a** to **TS-2**) is relaxed in the energy diagram of ZCu. The energy increase in **2a** can be attributed to the changes in geometry due to the presence of the zeolite surface since the geometry in **2a** without a zeolite surface is less stable than that in **2a** in Fig. 3 by about 20 kcal mol^{-1}. On the other hand, the energy changes in **1**, **TS-1** and **TS-2** indicate that the Cu^+ interacts with molecules differently when placed on the zeolite surface. It is obvious from the view of these transition state structures that this interaction affects the binding of O–1 to the Cu site. The change in the nature of the Cu–O bonding is most clearly seen in the structure **ZCuO**. The energy of this structure is closer to that of Cu^0 than that of Cu^+. The Cu–O binding energy is calculated as 51.9 kcal mol^{-1}, which should be compared with those calculated for Cu^0 and Cu^+, 30.1 and 60.1 kcal mol^{-1}, respectively. These results suggest that the enhanced catalysis of the ZCu is characterized by the change in oxygen affinity of Cu^+ due to the zeolite support. Cu^0 itself shows the highest oxygen affinity, but it is not an active catalyst because of the presence of the too stable complex **2a**. However, if the **2a** linear structure is not allowed as in ZCu owing to steric hindrance, **2a** becomes less stable. Then, the

Table 2 Energies of equilibrium and transition-state structures in the reaction $2NO \rightarrow N_2 + O_2$ over ZCu[a]

	1a[b]	1[b]	TS-1[b]	2a[b]	ZCuO + N_2O[b]	2b[b]	TS-2[b]	3a[b]	3b[b]	ZCu + N_2 + O_2[b]
This work—										
B3LYP[c]	−15.6	−20.1	−1.9	−22.1	−17.5	−21.6	17.6	−58.9	−57.3	−41.1
BP86[c]	−26.7	−39.7	−22.0	—	−32.0	—	−1.5	—	−65.0	−41.1
Schneider et al.[d]—										
BP86[e]	−19.6	−32.0	−25.3	—	−42.4	—	−5.9	—	−68.0	−45.2

[a] Energies are relative to the dissociation limit of two NO and ZCu (in kcal $mol)^{-1}$. [b] See Fig. 5 for the structures. [c] Basis sets: N and O, cc-pVDZ;[30] Cu, Si and Al, valence double-zeta basis set with effective core potential (1s–2p core) of Hay and Wadt;[31] H, (4s)/[1s] set in cc-pVDZ.[30] Cluster model: (SiH_3)–O–$Al(OH)_2$–O–$(SiH_3)^-$. See text for the computational details. [d] Ref. 18. [e] Basis sets: Cu, double-zeta s and p and triple-zeta d Slater-type functions; Al, N, O and H, double-zeta plus polarization Slater-type functions. Cluster model: $Al(OH)_4^-$.

barrier height on going from **2a** to **3a** becomes lower and the reaction proceeds more efficiently. Hence Cu^0 has the potential to be a highly active catalyst.

The changes in the nature of the Cu^+ are shown in the change of the electron population. The net charge of Cu^+ ranges from + 0.86 to + 1.19, which may corresponds to a changeable oxidation state of ZCu as suggested experimentally.[8,9] In the structures **TS-1**–**TS-2**, the electron population on the Cu^+ is depleted (net charge in the range + 1.14–1.19), and the lost electrons are transferred to the adsorbates. In addition a significant negative charge (0.14–0.25*e*) transfers from the cluster surface. As a result of these charge transfers, the adsorbates carry more negative charges of about − 0.4*e* in the structures **TS-1**–**TS-2**. The formation of such anionic species contributes to increasing the reactivity, as observed in the reaction over Cu^0.

The electronic interactions are investigated from insights into the populations in individual atomic orbitals. The notable features in the structures **TS-1**–**TS-2** are as follows: (i) the large population of 0.33–0.36*e* in Cu(4s); (ii) the diminished population of 1.51–1.58*e* in Cu($3d_{yz}$) (the *x*,*y*,*z* coordinate system is given in Fig. 5); and (iii) the large population of 1.49–1.65*e* in O1($2p_y$) which is in the range 1.10–1.23*e* for the system of the isolated Cu^+. These populations are entirely different from those of the isolated Cu^+. In addition to these changes, the Cu($3d_{z^2}$) populations are decreased to the same amount (0.05*e*) as in the isolated Cu^+. The population changes in Cu($3d_{yz}$) and O1($2p_y$) result from the formation of a π(d–p) bonding orbital. This π(d–p) bonding strengthens the Cu–O bonding and increases the anionic character of the adsorbed molecules in the zeolite. While this bonding is observed weakly in the complexes over the isolated Cu^+, it is much more enhanced in the zeolite environment. The large Cu(4s) populations are ascribed to the mixing of the Cu(4s) with the Cu($3d_{z^2}$) and orbitals of adsorbates composed mainly of the O1(p_z), as described in the case of isolated Cu^+ system, and with the orbitals of O_z.

It follows from these findings that the catalysis of ZCu is mainly due to the interaction with adsorbates through π(d–p) bonding. We suggest that the repulsion between the Cu($3d_{yz}$) and the lone pairs of the cluster oxygens plays an important role in producing the π(d–p) bonding. Analyses of the molecular orbitals revealed that the Cu($3d_{yz}$) mixes with the Cu($4p_y$) so that the electron density of the Cu($3d_{yz}$) is reduced in the cluster side and increased in the ligand side. This polarization is favorable for producing π(d–p) bonding between the Cu^+ and adsorbates and also for reducing the repulsion between Cu^+ and cluster oxygen.

It is well known that the binding of molecules to Cu^+ is affected very much by the number of attached molecules.[14–16,44–46] This means that the coordinated Cu^+ can bind another molecule more strongly than the isolated Cu^+. One example is the system of H_2O and Cu^+, for which it is known both experimentally[45] and theoretically[44,46] that the binding energy of the second H_2O is larger than that of the first. Another example of a close relation to our system is found in the study by Rodriguez-Santiago *et al.*,[47] who reported that the Cu^+ in the zeolite cluster model can bind an NO_2 molecule much more strongly than the isolated Cu^+. The mechanism of the first example is that the binding of the first H_2O (on the *z*-axis) induces an anisotropic change of the ionic radius of Cu^+ through hybrids of Cu^+(4s) and $Cu^+(3d_{z^2})$ with negative signs, and as a consequence the second H_2O can bind to the Cu^+ more strongly. The mechanism of the second example is the promotion of an electron from $Cu^+(3d_{xz})$ to Cu^+(4s) to reduce the repulsion between the $Cu^+(3d_{xz})$ and the lone pairs on the zeolite oxygen, and then the resulting $Cu^+(3d_{xz})$ hole and the occupied Cu^+(4s) interact with HOMO and SOMO, respectively, of NO_2. In our system, the first mechanism can be applied since the Cu(4s) and Cu($3d_{z^2}$) mix with negative signs. The presence of $Cu^+(3d_{xz})$ bonding in the second mechanism is common to our system.

4 Conclusion

We investigated theoretically the catalytic activity of Cu-exchanged zeolite for the decomposition of NO. We modelled the catalytic route by the reaction of two NO molecules to produce N_2 and O_2 over a Cu ion on a cluster model.

ZCu shows enhanced catalytic activity compared with the isolated Cu^+. The activity of ZCu as a catalyst is explained by the enhanced oxygen affinity and the ability to form anionic adsorbates. These chemical properties are entirely different from those of an isolated Cu^+. From the analysis of the electron populations in the individual atomic orbitals, it was found that one of the major interactions between the ZCu with adsorbates is the covalent π(d–p) bonding. The repulsion of the Cu(3d) with the electrons of the cluster oxygens benefits the π(d–p) bonding, which we suggest as the possible mechanism for the activation of the Cu^+ by the zeolite environment. Theory also suggests that Cu^0 could be an active catalyst if the reaction field is carefully prepared.

Acknowledgements

This research was financially supported by a grant from Genesis Research Institute Inc. and AGS project. N. Tajima and A. M. El-Nahas are indebted to the Japan Society for the Promotion of Science for research fellowships.

References

1 M. Iwamoto, S. Yokoo, K. Sakai and Kagawa, *J. Chem. Soc., Faraday Trans.*, 1981, **77**, 1629.
2 H. Yamashita, M. Matsuoka, K. Tsuji, Y. Shioya, M. Anpo and M. Che, *J. Phys. Chem.*, 1996, **100**, 397.
3 T. Beutel, J. Sárkány, G.-D. Lei, J. Y. Yan and W. M. H. Sachtler, *J. Phys. Chem.*, 1996, **100**, 845.
4 C. Lamberti, G. Spoto, D. Scarano, C. Pazé, M. Salvalaggio, S. Bordiga, A. Zecchina, G. T. Palomino and F. D'Acapito, *Chem. Phys. Lett.*, 1997, **269**, 500.
5 W. Grünert, N. W. Hayes, R. W. Joyner, E. S. Shpiro, M. R. H. Siddiqui and G. N. Baeve, *J. Phys. Chem.*, 1994, **98**, 10832.
6 H. Hamada, N. Matsubayashi, H. Shimada, Y. Kintaichi, T. Ito and A. Nishijima, *Catal. Lett.*, 1990, **5**, 189.
7 Y. Kuroda, H. Maeda, H. Moriwaki, N. Bamda and T. Morimoto, *Physica B*, 1989, **158**, 185.
8 Y. Li and K. Hall, *J. Catal.*, 1991, **129**, 202.
9 H.-J. Jang, W. K. Hall and J. L. d'Itri, *J. Phys. Chem.*, 1996, **100**, 9416.
10 M. Iwamoto, H. Yahiro, K. Tanaka, N. Mizuno, Y. Mine and S. Kagawa, *J. Phys. Chem.*, 1991, **95**, 3727.
11 A. W. Aylor, S. C. Larsen, J. A. Reimer and A. T. Bell, *J. Catal.*, 1995, **157**, 592.
12 M. Iwamoto, H. Yahiro, N. Mizuno, W.-X. Zhang, Y. Mine, H. Furukawa and S. Kagawa, *J. Phys. Chem.*, 1992, **96**, 9360.
13 J. Vaylon and W. K. Hall, *J. Phys. Chem.*, 1993, **97**, 1204.
14 W. F. Schneider, K. C. Hass, R. Ramprasad and J. B. Adams, *J. Phys. Chem.*, 1996, **100**, 6032.
15 K. C. Hass and W. F. Schneider, *J. Phys. Chem.*, 1996, **100**, 9292.
16 H. V. Brand, A. Redondo and P. J. Hay, *J. Phys. Chem. B*, 1997, **101**, 7691.
17 W. F. Schneider, K. C. Hass, R. Ramprasad and J. B. Adams, *J. Phys. Chem. B*, 1997, **101**, 4353.
18 W. F. Schneider, K. C. Hass, R. Ramprasad and J. B. Adams, *J. Phys. Chem. B*, 1998, **102**, 3692.
19 R. Ramprasad, K. C. Hass, W. F. Schneider and J. B. Adams, *J. Phys. Chem. B*, 1997, **101**, 6903.
20 B. L. Trout, A. K. Chakraborty and A. T. Bell, *J. Phys. Chem.* 1996, **100**, 4173.
21 B. L. Trout, A. K. Chakraborty and A. T. Bell, *J. Phys. Chem.* 1996, **100**, 17582.
22 M. J. Rice, A. K. Chakraborty and A. T. Bell, *J. Phys. Chem. A*, 1998, **102**, 7498.
23 Y. Yokomichi, T. Yamabe, H. Ohtsuka and T. Kakumoto, *J. Phys. Chem.*, 1996, **100**, 14424.

24 K. Teraishi, M. Ishida, J. Irisawa, M. Kume, Y. Takahashi, T. Nakano, H. Nakamura and A. Miyamoto, *J. Phys. Chem. B*, 1997, **101**, 8079.
25 D. Sülzle, H. Schwarz, K. H. Moock and J. K. Terlouw, *Int. J. Mass Spectrom. Ion Processes*, 1991, **108**, 269.
26 F. Haase and J. Sauer, *J. Am. Chem. Soc*., 1995, **117**, 3780.
27 H. van Koningsveld, *Acta Crystallogr., Sect. B*, 1990, **46**, 731.
28 A. D. Becke, *J. Chem. Phys*., 1993, **98**, 5648.
29 C. Lee, W. Yang, and R. G. Parr, *Phys. Rev. B*, 1988, **37**, 785; B. Miehlich, A. Savin, H. Stoll and H. Preuss, *Chem. Phys. Lett*., 1989, **157**, 200.
30 T. H. Dunning, Jr., *J. Chem. Phys*., 1989, **90**, 1007.
31 P. J. Hay and W. R. Wadt, *J. Chem. Phys*., 1985, **82**, 270.
32 A. E. Reed, R. B. Weinstock and F. Weinhold, *J. Chem. Phys*., 1985, **83**, 735.
33 M. J. Frisch, G. W. Trucks, H. B. Schlegel, P. M. W. Gill, B. G. Johnson, M. A. Robb, J. R. Cheeseman, T. A. Keith, G. A. Petersson, J. A. Montgomery, K. Raghavachari, M. A. Al-Laham, V. G. Zakrzewski, J. V. Ortiz, J. B. Foresman, J. Cioslowski, B. B. Stefanov, A. Nanayakkara, M. Challacombe, C. Y. Peng, P. Y. Ayala, W. Chen, M. W. Wong, J. L. Andres, E. S. Replogle, R. Gomperts, R. L. Martin, D. J. Fox, J. S. Binkley, D. J. Defrees, J. Baker, J. P. Stewart, M. Head-Gordon, C. Gonzalez and J. A. Pople, *GAUSSIAN 94*, *Revision E.1*, Gaussian, Pittsburgh, PA, 1995.
34 A. D. Becke, *Phys. Rev. A*, 1988, **38**, 3098.
35 J. P. Perdew, *Phys. Rev. B*, 1986, **33**, 8822.
36 C. Møller and M. S. Plesset, *Phys. Rev*., 1934, **46**, 618.
37 B. S. Jursic, *Chem. Phys. Lett*., 1995, **236**, 206; A. L. L. East, *J. Chem. Phys*., 1998, **109**, 2185.
38 H. A. Duarte, E. Proynov and D. R. Salahub, *J. Chem. Phys*., 1998, **109**, 26.
39 S. G. Kukolich, *J. Mol. Spectrosc*., 1983, **98**, 80.
40 A. W. R. McKellar, J. K. G. Watson and B. J. Howard, *Mol. Phys*., 1995, **86**, 273.
41 B. J. Howard and A. R. W. McKellar, *Mol. Phys*., 1993, **78**, 55.
42 J. R. Hetzler, M. P. Casassa and D. S. King, *J. Phys. Chem*., 1991, **95**, 8086.
43 G. Herzberg, *Molecular Spectra and Molecular Structure*, *III. Electronic Spectra and Electronic Structures of Polyatomic Molecules*, Van Nostrand, New York, 1966.
44 A. M. El-Nahas, N. Tajima and K. Hirao, *J. Mol. Struct*. (*THEOCHEM*), 1999, **469**, 201.
45 T. F. Magnera, D. E. David, D. Stuhlik, R. G. Orth, H. T. Jonkman and J. Michl, *J. Am. Chem. Soc*. 1989, **111**, 5036.
46 C. W. J. Bauschlicher, S. R. Langhoff and H. Partridge, *J. Chem. Phys*., 1991, **94**, 2068.
47 L. Rodriguez-Santiago, M. Sierka, V. Branchadell, M. Sodupe and J. Sauer, *J. Am. Chem. Soc*., 1998, **120**, 1545.

Paper 9/03383A